


國立交通大學

電機與控制工程學系

碩士論文

一種使用啾聲轉換演算法為頻率擷取並應  
用在 GPS 接收器的新型快速方法



A NEW FAST FREQUENCY-ACQUISITION  
TECHNIQUE USING CHIRP TRANSFORM  
ALGORITHM FOR GPS RECEIVER

研 究 生：吳嘉富

指導教授：鄭木火博士

中華民國九十四年七月

一種使用啾聲轉換演算法為頻率擷取並應用在  
GPS 接收器的新型快速方法

A NEW FAST FREQUENCY-ACQUISITION  
TECHNIQUE USING CHIRP TRANSFORM  
ALGORITHM FOR GPS RECEIVER

研 究 生：吳嘉富

Student : Jia-Fu Wu

指導教授：鄭木火博士

Advisor : Mu-Huo Cheng



A Thesis  
Submitted to Department of Electrical and Control Engineering  
College of Electrical Engineering and Computer Science  
National Chiao Tung University  
In Partial Fulfillment of the Requirements  
for the Degree of Master  
in Electrical and Control Engineering  
July 2005  
Hsinchu, Taiwan, Republic of China

中華民國九十四年七月

# 一種使用啾聲轉換演算法為頻率擷取並應用在 GPS 接收器的新型快速方法

研究生: 吳嘉富

指導教授: 鄭木火博士

國立交通大學電機與控制工程學系

## 摘要

訊號擷取在全球定位系統 (GPS) 接收器中是一個粗略的同步過程, 其目的是估測偽隨機碼 (Pseudo-Random Number, PRN) 的延遲和都普勒頻率。既有文獻中的擷取方法可分為時域法和頻域法。早期的方法是在時域中計算相關函數以達到最大近似估測。近年來擷取的方法使用快速傅立葉轉換法 (Fast Fourier Transform, FFT) 在頻域中計算相關函數以減少所需計算複雜度。但即使是使用頻域法若要估測到幾十赫芝解析度之都普勒頻率, 其所需的計算複雜度仍相當高。此乃因為 FFT 是計算訊號整個頻譜, 但所要的都普勒頻率範圍相對於訊號的頻譜來說相當的小。本論文因此提出利用啾聲轉換演算法 (Chirp Transform Algorithm, CTA) 的方法來克服此問題。主要是利用 CTA 會將所有的運算功能均放在都普勒頻率的頻段上, 故可降低計算複雜度或提高頻率解析度。本論文並將以 CTA 估測都普勒頻率及以 FFT 估測 PRN 碼的相位兩方法相結合, 形成一新的訊號擷取方法, 稱之為兩階段法。其與傳統方法相比較, 計算複雜度在同一性能下將可降低。本論文最後以運算複雜度為量測參數, 使用電腦模擬來驗證本論文所提方法之優越性。

**關鍵詞:** 全球定位系統、假隨機碼、傅立葉轉換法、啾聲轉換演算法。

# A NEW FAST FREQUENCY-ACQUISITION TECHNIQUE USING CHIRP TRANSFORM ALGORITHM FOR GPS RECEIVER

Student: Jia-Fu Wu      Advisor: Dr. Mu-Huo Cheng

Institute of Electrical and Control Engineering  
National Chiao-Tung University

## Abstract

Signal acquisition in GPS receiver is a coarse synchronization process whose goal is to estimate the Pseudo-Random Number (PRN) code delay and the Doppler frequency. The acquisition methods, in literatures, are performed in either time domain or frequency domain. Early methods compute the correlation in the time domain to achieve the performance of maximum likelihood estimation (MLE). Recently, new realization techniques have been developed for computing the correlation in frequency domain via the fast Fourier transform (FFT) such that the computation complexity is significantly reduced. The approaches via the FFT, however, still require high computation complexity if one desires to estimate the Doppler frequency with its resolution up to a few Hertz. The reason is because the FFT evaluates the whole signal spectrum, but the range of possible Doppler frequency is relatively much small compared with the signal spectrum. Therefore, this thesis employs the Chirp Transform Algorithm (CTA) to overcome this drawback because the CTA evaluates only within the range of Doppler frequency. This approach can either reduce the computation complexity or increase the frequency resolution. In this thesis, we further combine together the two techniques, one using the CTA for Doppler frequency estimation and the other using the FFT for code delay estimation, yielding a new acquisition approach, referred to as the two-stage search method which, compared with traditional methods, can reduce the computation complexity. Computer simulations are also performed to demonstrate the advantages of our proposed methods.

**Keywords:** GPS, C/A, PRN, FFT, CTA.

# 誌謝

此論文能順利完成，要特別真誠地感謝我的指導教授鄭木火教授，在這短短的兩年研究生涯中，無論是待人接物的誠懇真摯或治學態度的嚴謹細心，均使我在生活及學識上獲益良多。因此在本論文付梓之際，對於辛勤傳道授業的老師致上最誠摯的謝意。

在口試期間承蒙林清安教授和張志永教授撥空指正並提供許多寶貴的意見。在此感謝你們的辛勞。同時感謝畢業學長再生、逸帆、琪展、鈞哲、政衛、立峰，以及實驗室的所有成員：天貴、國偉、佩樺、振杰、浩緯、信良、俊維、啓峰在課業上的切磋討論及生活上的歡聲笑語，為平靜單調的研究生活增添不少色彩，也要感謝室友峻永、柏壽、群棋、召漢、進元和許多好友時時給我鼓勵與幫助。

最後要感謝我的家人，由於他們的付出和不斷地鼓勵，讓我能無後顧之憂的從事研究，順利完成學業，並且有能力面對下一波的困難與挑戰。



# TABLE OF CONTENTS

<b>ABSTRACT IN CHINESE</b>	<b>i</b>
<b>ABSTRACT IN ENGLISH</b>	<b>ii</b>
<b>ACKNOWLEDGEMENTS IN CHINESE</b>	<b>iii</b>
<b>LIST OF FIGURES</b>	<b>vi</b>
<b>LIST OF TABLES</b>	<b>viii</b>
<b>1 INTRODUCTION</b>	<b>1</b>
1.1 Introduction . . . . .	1
1.2 Motive and Literatures Review . . . . .	1
1.3 Organization of the Thesis . . . . .	2
<b>2 GPS SIGNAL MODEL</b>	<b>3</b>
2.1 Introduction to GPS . . . . .	3
2.2 GPS Signals From Satellites . . . . .	4
2.2.1 Signal Structure . . . . .	4
2.2.2 Generation of C/A Code . . . . .	4
2.3 GPS Receiver . . . . .	6
2.3.1 RF Module . . . . .	7
2.3.2 A/D Converters . . . . .	8
2.4 Input Signals of The Digital Baseband Processor . . . . .	8
<b>3 C/A CODE ACQUISITION</b>	<b>9</b>
3.1 Acquisition Using FFT . . . . .	10
3.1.1 Serial(code delay)-Parallel(Doppler frequency) Method . . . . .	10

3.1.2	Parallel(code delay)-Serial(Doppler frequency) Method . . . . .	11
3.2	Acquisition Using CTA . . . . .	12
3.2.1	CTA Algorithm [13] . . . . .	13
3.2.2	CTA Method . . . . .	14
3.2.3	Two-stage Search Strategy . . . . .	15
3.3	Computation Complexity . . . . .	17
<b>4</b>	<b>SIMULATIONS AND DISCUSSIONS</b>	<b>20</b>
<b>5</b>	<b>CONCLUSIONS</b>	<b>29</b>
	<b>References</b>	<b>30</b>



# LIST OF FIGURES

Fig. 2.1 C/A code generator . . . . .	5
Fig. 2.2 Autocorrelation of satellite 19 . . . . .	5
Fig. 2.3 Crosscorrelation of satellites 19 and 31 . . . . .	6
Fig. 2.4 Spectrum of a C/A code . . . . .	6
Fig. 2.5 The block diagram of GPS receiver and DSP . . . . .	7
Fig. 2.6 RF Module . . . . .	7
Fig. 3.1 Two-dimensional C/A code search region . . . . .	9
Fig. 3.2 Acquisition system block diagram . . . . .	10
Fig. 3.3 Using FFT to estimate the Doppler frequency . . . . .	11
Fig. 3.4 Using FFT to estimate the code delay . . . . .	12
Fig. 3.5 Frequency samples for CTA . . . . .	13
Fig. 3.6 Block diagram of CTA . . . . .	14
Fig. 3.7 Using CTA to estimate the Doppler frequency . . . . .	15
Fig. 3.8 Block diagram of CTA using FFT . . . . .	15
Fig. 3.9 Two-stage search strategy diagram . . . . .	16
Fig. 4.1 Received signal in baseband from the satellite 12 with $C/N_0 = 40$ dB-Hz. . . . .	20
Fig. 4.2 Using the conventional method from the satellite 12 with $C/N_0 = 40$ dB-Hz : 3-dimensional view . . . . .	21
Fig. 4.3 Using the conventional method from the satellite 12 with $C/N_0 = 40$ dB-Hz : lateral view . . . . .	21
Fig. 4.4 Using the conventional method from the satellite 12 with $C/N_0 = 40$ dB-Hz : lateral view 2 . . . . .	22



Fig. 4.5 Using FFT to estimate the Doppler frequency from the satellite 12 with $C/N_0 = 40$ dB-Hz : 3-dimensional view . . . . .	22
Fig. 4.6 Using FFT to estimate the Doppler frequency from the satellite 12 with $C/N_0 = 40$ dB-Hz : lateral view . . . . .	23
Fig. 4.7 Using FFT to estimate the Doppler frequency from the satellite 12 with $C/N_0 = 40$ dB-Hz : lateral view 2 . . . . .	23
Fig. 4.8 Using FFT to estimate the code delay from the satellite 12 with $C/N_0 = 40$ dB-Hz : 3-dimensional view . . . . .	24
Fig. 4.9 Using FFT to estimate the code delay from the satellite 12 with $C/N_0 = 40$ dB-Hz : lateral view . . . . .	24
Fig. 4.10 Using FFT to estimate the code delay from the satellite 12 with $C/N_0 = 40$ dB-Hz : lateral view 2 . . . . .	25
Fig. 4.11 Using CTA to estimate the Doppler frequency from the satellite 12 with $C/N_0 = 40$ dB-Hz : 3-dimensional view . . . . .	25
Fig. 4.12 Using CTA to estimate the Doppler frequency from the satellite 12 with $C/N_0 = 40$ dB-Hz : lateral view . . . . .	26
Fig. 4.13 Using CTA to estimate the Doppler frequency from the satellite 12 with $C/N_0 = 40$ dB-Hz : lateral view 2 . . . . .	26
Fig. 4.14 Using two-stage search from the satellite 12 with 77 coarse frequency bins $C/N_0 = 40$ dB-Hz : 3-dimensional view . . . . .	27
Fig. 4.15 Using Two-Stage search from the satellite 12 with 77 coarse frequency bins $C/N_0 = 40$ dB-Hz : lateral view . . . . .	27
Fig. 4.16 Using Two-Stage search from the satellite 12 with 77 coarse frequency bins $C/N_0 = 40$ dB-Hz : lateral view 2 . . . . .	28
Fig. 4.17 Using CTA to estimate the Doppler frequency with the correct code delay from the satellite 12 $C/N_0 = 40$ dB-Hz. . . . .	28

# LIST OF TABLES

Table 3.1	Computation complexity of all . . . . .	18
Table 3.2	Common parameters . . . . .	18



## Chapter 1

# INTRODUCTION

### 1.1 Introduction

Global Positioning System (GPS) receivers must acquire and track the PRN code from several GPS satellites. In order to track and decode the navigation data in the received signal, an acquisition process must be first done to detect the presence of the signal. Once the signal is detected, the necessary parameters which are the PRN code delay and the Doppler frequency must be obtained and passed to a tracking program. From the tracking program the navigation data can be obtained. The tracking effort can be greatly reduced if the initial code delay and the Doppler frequency are more accurate. This thesis presents a new and efficient method to increase the accuracy of the Doppler frequency acquisition. In our proposed method, we find that it is easy to increase frequency resolution up to the level of the bandwidth of tracking loop with lower computation complexity. So, one can also combine our method with other fast methods which are good at finding code phase/delay fast, such as FFT. Thus, a two-stage search strategy is proposed in this thesis. In this way, not only can the burden of tracking loop be alleviated, but also the computation complexity of acquisition can be reduced.

### 1.2 Motive and Literatures Review

Although GPS signal acquisition is a mature subject, there is still some ways to improve acquisition on computation complexity. Acquisition is the most time-consuming operation in the GPS receiver. A fast search algorithm was presented by Cheng in [1]; it is using FFT to find the Doppler frequency. In this thesis, we refer to this method as to Serial (code delay)-Parallel (Doppler frequency) Method, meaning that it is performed by doing serial code correlation along with searching the Doppler frequency in the spectrum. Another fast

search algorithm was presented by Van Nee in [2][5][6]; it is also using the FFT to search code delays, instead of Doppler frequency. We call this approach Parallel-Serial method. The idea of Serial-Parallel method is adopted by [3][4] for solving the problem of large Doppler frequency in the earth orbit satellites (LEOS) channel. In the methods discussed above, they still have much computation to do as a result of long acquisition intervals if they want to find fine frequency resolution. In reference [7], they propose a new algorithm based on the stochastic nonlinear filtering framework, and they claim that the proposed architecture yields small code/frequency acquisition intervals and reduced tracking errors. However, it appears to be complicated, and its estimation of frequency range depends on SNR ( $C/N_0$ ). In our proposed method, we can dramatically increase frequency resolution under the same SNR with a little increment of complexity. In the book [8], it uses Serial-Parallel method and employs the phase relation to find fine frequency resolution. To reduce the complexity, the book presents an approach to multiply the delay of the received signal with the no-delay one to eliminate the carrier frequency first. It can operate faster than the FFT method, but it requires a higher SNR.

### 1.3 Organization of the Thesis

The remainder of this thesis is divided into four chapters including conclusions. Chapter 2 reviews the GPS, its receiver structure, and the baseband signal. Chapter 3 illustrates the differences of two fast current methods and our methods. Chapter 4 demonstrates the computer simulations and lists of computation complexity. The final chapter is the conclusions.

## Chapter 2

# GPS SIGNAL MODEL

### 2.1 Introduction to GPS

GPS is a space-based radionavigation system which is managed for the Government of the United States by the U.S. Air Force (USAF), the system operator. The GPS is designed to provide precise position, velocity and timing information on a global common coordinate system to an unlimited number of suitably equipped users. It consists of three segments: the space-segment, the control-segment, and the user-segment. When fully deployed, the space-segment will contain 21 primary space vehicles and 3 spares in 12-hour,  $55^\circ$  inclination orbits with 4 space vehicles distributed in each of 6 planes. The control-segment consists of monitor stations to check the health of the satellites, to determine their orbits and the behavior of their atomic clocks, and to inject the broadcast message into the satellites. The user-equipment is the key for users to access the system which has undergone extensive development since the GPS concept was initiated in 1973.

Normally for a user to determine his absolute position, he needs to receive signals from four different GPS satellites. A GPS satellite transmits information to users on two different L-band frequencies L1 and L2. Both L1 and L2 signals are also continuously modulated with the navigation data bit stream at 50 bit per second.

The signals are modulated with two PRN codes : Precision (P) code and Coarse/Acquisition (C/A) code. The actual P code is not directly transmitted by the satellite, but it is modulated by a Y code, which is often referred to as the P(Y) code. In general, in order to acquire the P(Y) code, the C/A code is usually acquired first. Thus, if one wants to get the signal from satellites, one must demodulate the received signal to obtain the C/A code first.

Therefore, in this thesis we only focus on the acquisition of C/A code.

## 2.2 GPS Signals From Satellites

### 2.2.1 Signal Structure

The GPS signal contains two frequency components: link 1 (L1) and link 2 (L2). The center frequency of L1 is at 1575.42 MHz and L2 is at 1227.6 MHz. These frequencies are coherent with a 10.23 MHz clock. These frequencies are very accurate as their reference is an atomic frequency. The signal structure of the satellite is well defined in [9]. The L1 frequency is Bipolar-Phase Shift Key (BPSK) modulated by the composite C/A code and navigation data bit train if one only considers the C/A part, and it can be written as:

$$S(t) = AP(t)D(t)\sin(w_1t + \phi) \quad (2.1)$$

where  $D(t)=\pm 1$  represents the data code,  $w_1$  is the L1 frequency,  $\phi$  is the initial phase.  $A$  is the amplitude of the C/A code, and  $P(t)=\pm 1$  represents the phase of the C/A code.

### 2.2.2 Generation of C/A Code

The characteristics of the C/A code are all defined in [9], which defines its structure and the basic method used for generating it. The C/A code consists of 1.023 Mbps  $P_i(t)$  patterns with Modulo 2 addition of the navigation data bit train,  $D(t)$ , which is clocked at 50 bps. The resultant composite bit train is then used to BPSK modulate the L-band carrier. The user receiver is then required to independently generate and synchronize with the satellite transmitted C/A code and perform Modulo 2 addition in order to decode and interpret the navigation message. The linear  $P_i(t)$  pattern (C/A-code) is the Modulo-2 sum of two 1023-bit linear patterns,  $G_1$  and  $G_2$ . The latter sequence is formed by effectively delaying the  $G_2$  sequence by an integer number of chips from 5~950 to produce 36 unique  $P(t)$  patterns (listed in [9]). The  $G_1$  and  $G_2$  sequences are generated by 10-stage shift registers having the following polynomials as referred to in the shift register input.

$$G_1 : x^{10} + x^3 + 1$$

$$G_2 : x^{10} + x^9 + x^8 + x^6 + x^3 + x^2 + 1$$

The initialization vector for the G1 and G2 sequences is (1111111111). The effective delay of the G2 sequence to form the  $G_{2i}(t)$  sequence is accomplished by combining the output of two stages (S1 and S2) of the G2 shift register by Modulo-2 addition. This allows the generation of 36 unique C/A(t) code phases using the same basic code generator as shown in Fig. 2.1.

Three Figures 2.2, 2.3, and 2.4 can describe the characteristics of C/A code [15].

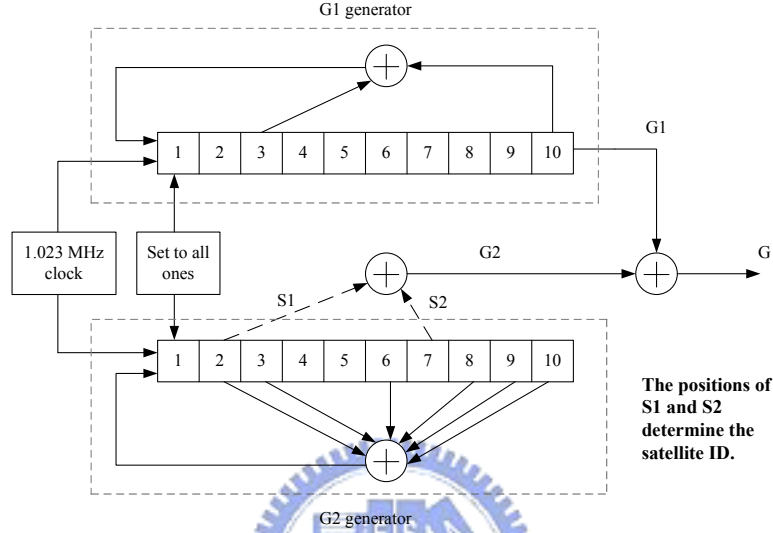


Fig. 2.1: C/A code generator

Fig. 2.2 is the autocorrelation of satellite 19. The the maximum peak is 1023 whose position is deliberately shifted to the center of the figure for a clear view. The rest of the correlation has three values 63, -1, 65.

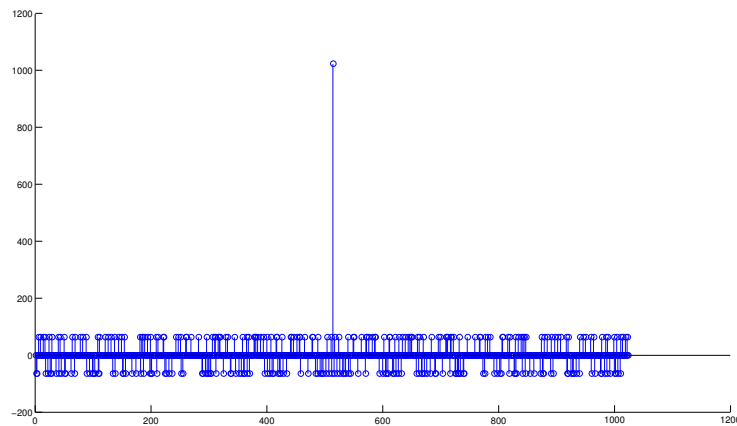


Fig. 2.2: Autocorrelation of satellite 19

Fig. 2.3 is the crosscorrelation of satellites of 19 and 31. It also has three values 63, -1, -65. Figure 2.4 is the spectrum of C/A code satellite 12.

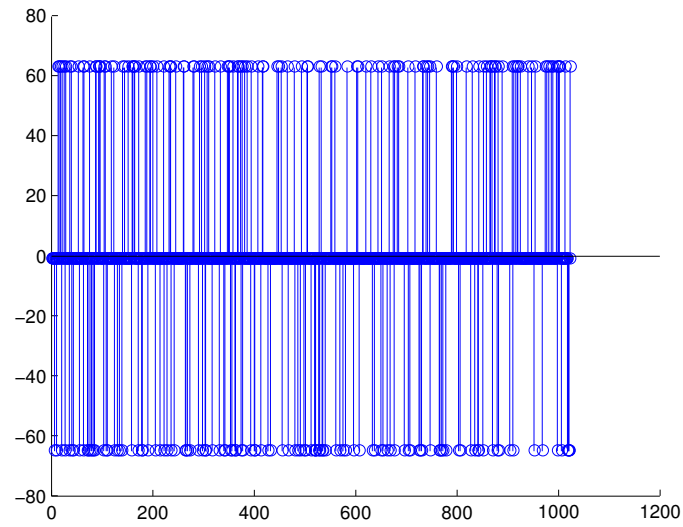


Fig. 2.3: Crosscorrelation of satellites 19 and 31

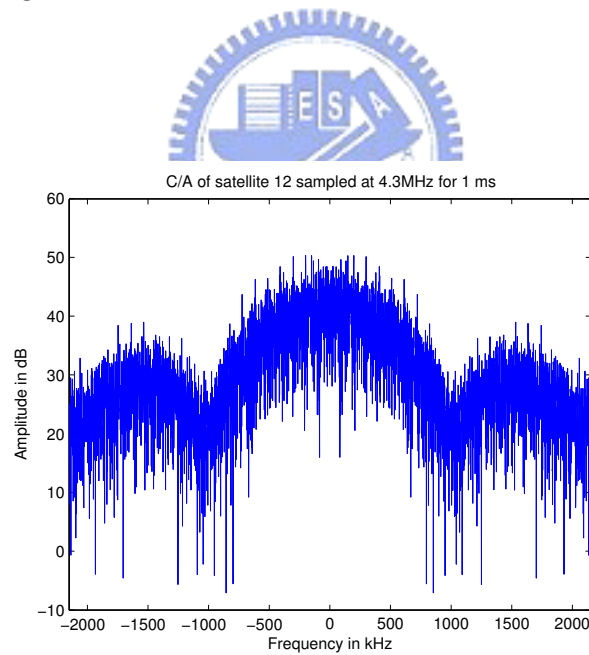


Fig. 2.4: Spectrum of a C/A code

## 2.3 GPS Receiver

A GPS receiver simply consists of two parts : RF module and A/D convert. The RF signals from the antenna are converted to the baseband signals in the RF module. The RF



module consists of a mixer and a lowpass (LP) filter. A/D convert is to digitize the analog baseband signal for the digital signal processor (DSP) to process. They are shown in Fig. 2.5.

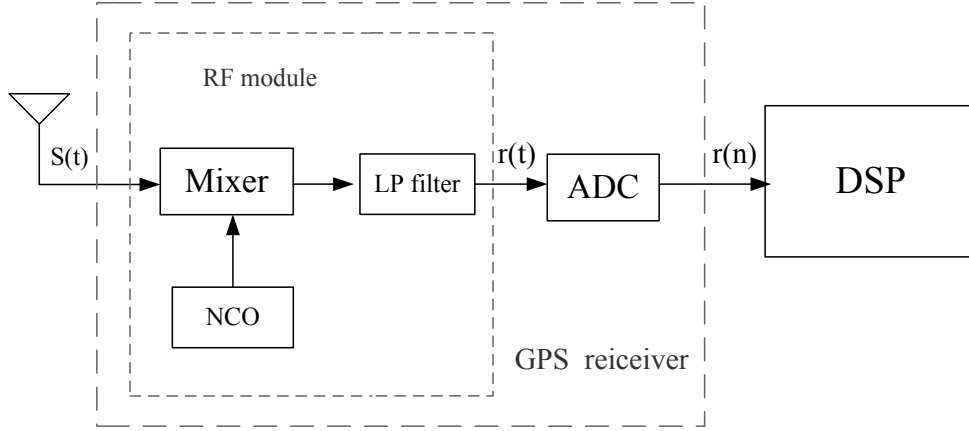


Fig. 2.5: The block diagram of GPS receiver and DSP

### 2.3.1 RF Module

Because of the uncertainty of the Doppler frequency in the L1 signals (varying from -5 kHz to +5 kHz for static receivers), the center frequency of the baseband carrier,  $w_c$ , should be 5 kHz or large for accurately estimating the Doppler frequency in the digital baseband. A baseband carrier frequency of 17.248 kHz is chosen for the L1 channels [10]. With a simple single stage downconverter, the local NCO generates RF signals of (1575.42 MHz-17.248 kHz) for the L1 channel. Fig. 2.6 depicts the block diagram of the RF module.

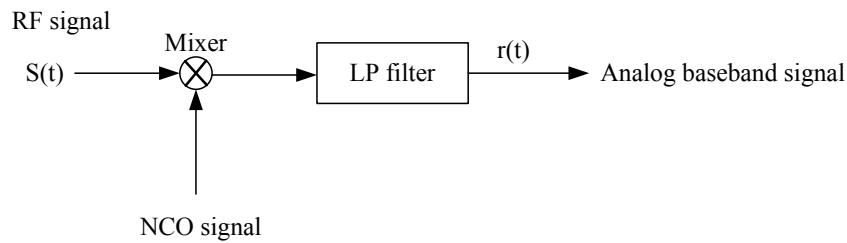


Fig. 2.6: RF Module

The bandwidth of the low-pass (LP) filter is determined by the C/A code power spectrum density, which varies with a  $Sinc^2(kf)$  form in an amplitude level as shown in Figure 2.4. The baseband signal from the RF module is fed to the A/D converter, which samples the

signals and outputs the corresponding discrete baseband signals.

### 2.3.2 A/D Converters

According to the sampling theorem [13], a signal may be reconstructed without error from regularly spaced samples taken a rate  $f_s$ , which is at least twice the maximum frequency  $f_m$  present in the signal. Therefore, the sampling rate for the baseband C/A signal should be

$$f_s \geq 2 \times 1.023 \text{ MHz} = 2.046 \text{ MHz} \quad (2.2)$$

High sampling rate requires higher realization complexity. A lower sampling rate will yield estimates with lower time resolution. The time resolution is too coarse to position. In reference [10], a low sampling rate  $f_s = 2.1518 \text{ MHz}$  under which the commensurability error can be reduced to a negligible level [13] is adopted in this thesis.

## 2.4 Input Signals of The Digital Baseband Processor

Because the period of navigation data is very long compared with C/A code, one can ignore it within the acquisition time. The input signal plus noise in a single channel can be modeled [10][11] as :

$$r(n) = AP[(1 + \zeta)nT_s - \varepsilon T_p]e^{j(w_b + w_d)n + \phi_0} + N(n), \quad (2.3)$$

where  $P[\cdot]$  is a  $\pm 1$  - valued C/A code, delayed by  $\tau = \varepsilon T_p$  with respect to GPS system time,  $N(n)$  is the Gaussian white noise,  $w_b = 2\pi f_b T_s$  and  $w_d = 2\pi f_d T_s$  are the digital radian frequencies corresponding to the baseband carrier  $f_b$  and Doppler frequency  $f_d$ ,  $T_s$  is the sampling period,  $T_p$  is the code chip width, and  $\phi_0$  is the initial carrier phase at  $n=0$ . Here, we define the carrier frequency  $w_c = w_b + w_d$ . The baseband carrier  $f_b$  is known as 17.248 kHz. If one wants to know the Doppler frequency, he can obtain it from the carrier frequency,  $w_c$ .

## Chapter 3

# C/A CODE ACQUISITION

In estimation theory, acquisition is to find code delay,  $m$ , and carrier frequency,  $w_c$ , to make the likelihood function maximized. It is the well-know mathematical approach, Maximum Likelihood Estimate (MLE). The likelihood function for acquisition is written as:

$$L(m, w_c) = \frac{1}{N_0} \left| \sum_{n=0}^{N-1} r(n)p(n+m) \cos(w_c n) \right|^2 + \frac{1}{N_0} \left| \sum_{n=0}^{N-1} r(n)p(n+m) \sin(w_c n) \right|^2 \quad (3.1)$$

where  $N$  is the length of observation interval,  $r(n)$ ,  $N_0$  is the power spectral density of the noise,  $N(n)$ , and  $w_c$  is the carrier frequency which is defined in section 2.4. The equation is derived [11][12] under over a sufficiently short observation interval the signal parameters may be viewed as constant and the noise is Gaussian white. From the equation (3.1), one can find the computation complexity of the likelihood function is dominated by the inner part of the brackets. Usually, it is called correlation or crosscorrelation. Because we must change the possible values,  $m$  and  $w_c$ , to make  $L$  maximized, acquisition can be thought of as a 2-dimension search process  $(m, w_c)$  in a uncertainty region shown in Fig. 3.1.

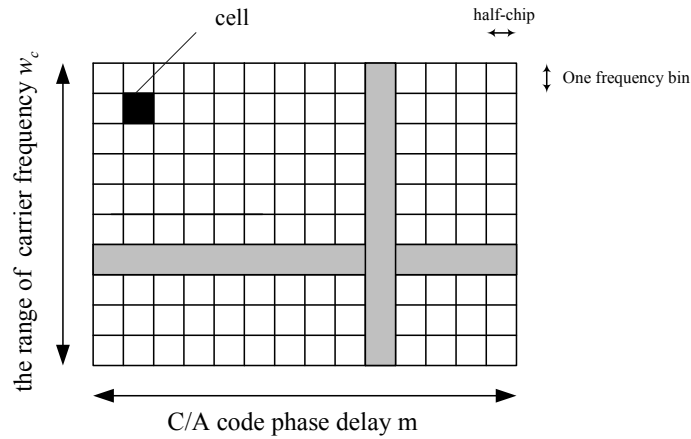


Fig. 3.1: Two-dimensional C/A code search region

Each cell represents the different value of  $(m, w_c)$ . The range and resolution of region depends

on the environments or applications. Usually, for static receivers the range of Doppler frequency is  $-5 \text{ kHz} \sim 5 \text{ kHz}$ , and that of code delay is the period of the code. Intuitively, one can move cell by cell to find the maximum value of  $L$ . The correct cell is identified by measurement of the output power of the correlators as shown in Fig. 3.2. The signal is detected until the maximum power is found or the power exceeds the predetermined threshold as shown in Fig. 3.2. Usually, this method is called the conventional method. However, one can fix a certain parameter to find another one along a row or column as shown in Fig.3.1. Since the strategy searching along the row or column can be performed with FFT, they are called FFT methods. In the following sections, FFT methods will be discussed first, and our methods will be introduced.

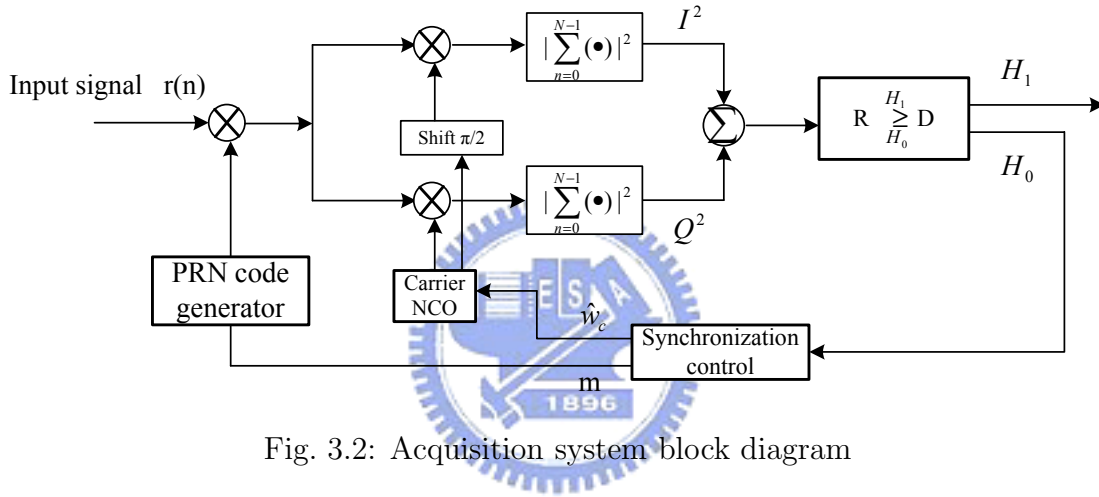


Fig. 3.2: Acquisition system block diagram

### 3.1 Acquisition Using FFT

In literatures, many methods [1][2][3][4][5][6][8] employ FFT to reduce computation complexity. In this section, we review these methods, show they can be implemented by FFT in mathematical derivation, and the steps of implementation .

#### 3.1.1 Serial(code delay)-Parallel(Doppler frequency) Method

The method is to delay the code and then to find the Doppler frequency with FFT in parallel. Then the found frequency is took back to compute the correlation power. So in this thesis, we call this method as Serial-Parallel method, or simply S-P method. The detailed process is shown in Fig. 3.3. After applying FFT, for finding the Doppler frequency in the signal spectrum one can only do  $R_w$  multiplications, instead of  $N$  multiplications, to reduce the

computation complexity.  $R_w$  is the number of frequency samples on the range of Doppler frequency.

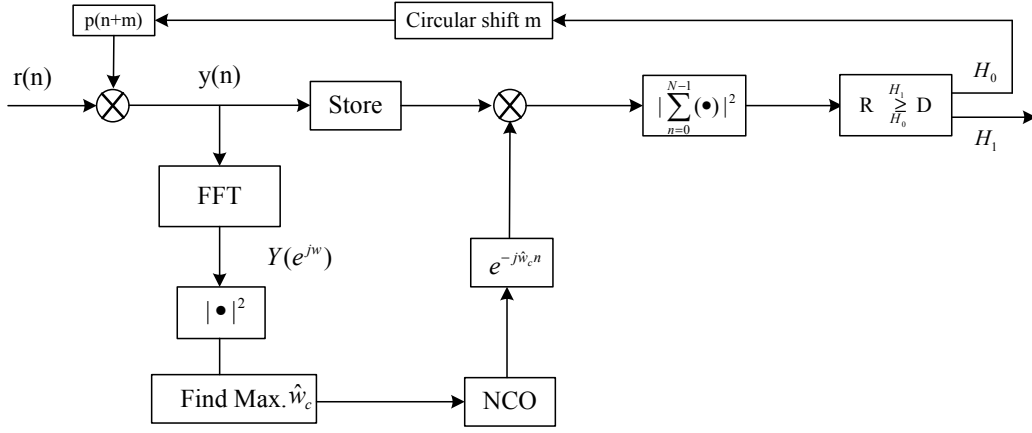


Fig. 3.3: Using FFT to estimate the Doppler frequency

### 3.1.2 Parallel(code delay)-Serial(Doppler frequency) Method

The two inner part of brackets in equation (3.1) can also be written below.

$$y(m) = \sum_{n=0}^{N-1} r(n)p(m+n)e^{-jw_c n} \quad (3.2)$$

If one fixes the carrier frequency  $w_c$  as  $w$ , then the equation (3.2) becomes the correlation of  $r(n)e^{-jwn}$  and  $p(n)$ . It is similar to search the code delay in parallel and change  $w_c$  in serial, so it is called as Parallel-Serial method, or simply P-S method. Because the C/A code repeats each 1 ms, it is a circular signal. One can use FFT and IFFT to compute  $y$  to reduce the computation complexity. Apply FFT to  $y(m)$

$$\begin{aligned} Y(k) &= \sum_{m=0}^{N-1} y(m)e^{-j\frac{2\pi km}{N}} \\ &= \sum_{m=0}^{N-1} \sum_{n=0}^{N-1} r(n)p(m+n)e^{-jwn}e^{-j\frac{2\pi km}{N}} \\ &= \sum_{n=0}^{N-1} r(n) \sum_{m=0}^{N-1} p(m+n)e^{-j\frac{2\pi km}{N}}e^{-jwn} \\ &= \sum_{n=0}^{N-1} r(n) \sum_{m=0}^{N-1} p(m+n)e^{-j\frac{2\pi k(m+n)}{N}}e^{j\frac{2\pi kn}{N}}e^{-jwn} \\ &= \sum_{n=0}^{N-1} r(n)P(k)e^{j\frac{2\pi kn}{N}}e^{-jwn} \end{aligned}$$

$$= P(k) \left[ \sum_{n=0}^{N-1} r(n) e^{-jwn} e^{j\frac{2\pi kn}{N}} \right] \quad (3.3)$$

From (3.3), one can find that the FFT of equation (3.2) is the multiplication of the FFT of  $p(n)$  and the IFFT of  $Nr(n)e^{-jwn}$ . The result of equation (3.3) is based on the circular property of  $p(n)$ , and  $r(n)$  need not have this property. In practice,  $r(n)$  can not be considered as circular, because it contains noise even if  $r(n)$  also contains the circular C/A code,  $p(n)$ . However, some methods, like reference [8], which also apply FFT to estimate code delays assume that the multiplication of  $p(m+n)$  and  $e^{-jwn}$  is circular. Under the above assumption, the obtained likelihood function with the right estimated parameters will be smaller than us. In other words, when SNR is very low, these methods with the above assumption can not detect the wanted signal efficiently and sensitively. After getting  $y$ , we can compute  $L$  to determine whether the signal is detected. In summary, the block diagram shown in Figure 3.4 is equivalent to that shown in Fig 3.2.

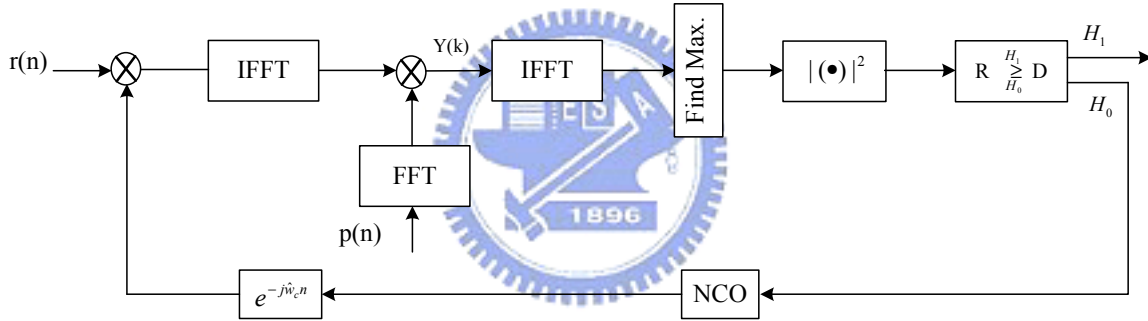


Fig. 3.4: Using FFT to estimate the code delay

## 3.2 Acquisition Using CTA

In this section, the Chirp Transform Algorithm(CTA) is introduced and illustrated how we can employ it to increase frequency resolution within the range of the Doppler frequency and to reduce computation complexity. In the common FFT methods, the frequency resolution obtained from 1 ms of data is 1 kHz, which is too coarse for the tracking loop. The desired frequency resolution [8] should be within a few tens of Hertz. Usually, the tracking loop has a width of only a few Hertz. Using FFT to find fine resolution is not an appropriate approach, because in order to achieve 10 Hz resolution we must apply FFT to 100 ms of

data which is 215200 samples at the sampling frequency 2.1518 MHz. Therefore, it is too time-consuming for FFT operation.

### 3.2.1 CTA Algorithm [13]

The CTA is more flexible than the FFT, since it can be used to compute any set of equally spaced samples of the Fourier transform on the unit circle, as indicated in Fig. 3.5.

To derive the CTA, we let  $y[n]$  denote an  $N$ -sequence and  $Y(e^{jw})$  its Fourier transform.

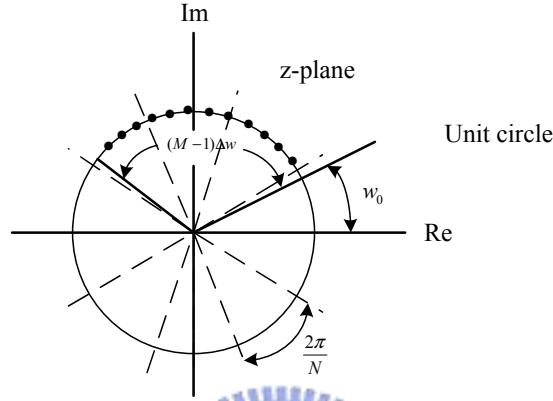


Fig. 3.5: Frequency samples for CTA

We consider the evaluation of  $M$  samples of  $Y(e^{jw})$  from an initial frequency  $w_0$  by the increment  $\Delta w$  which can be chosen arbitrarily. Thus, DFT is simply the special case of CTA when  $w_0 = 0$ ,  $M = N$ , and  $\Delta w = 2\pi/N$  which is also shown in Fig. 3.5. The detailed derivation [13] is shown below.

$$\begin{aligned}
 Y(e^{jw_k}) &= \sum_{n=0}^{N-1} y(n)e^{-jw_k n}, \quad (w_k = w_0 + k\Delta w, \quad k = 0, 1, \dots, M-1) \\
 &= \sum_{n=0}^{N-1} y(n)e^{-j(w_0 + k\Delta w)n}, \quad (\text{Define } W = e^{-j\Delta w}) \\
 &= \sum_{n=0}^{N-1} y(n)e^{-jw_0 n} W^{kn}, \quad (kn = \frac{n^2 + k^2 - (k-n)^2}{2}) \\
 &= \sum_{n=0}^{N-1} y(n)e^{-jw_0 n} W^{[n^2 + k^2 - (k-n)^2]/2} \\
 &= \sum_{n=0}^{N-1} y(n)W^{-(k-n)^2/2} e^{-jw_0 n} W^{(n^2 + k^2)/2} \\
 &= W^{k^2/2} \sum_{n=0}^{N-1} y(n)e^{-jw_0 n} W^{n^2/2} W^{-(k-n)^2/2}
 \end{aligned}$$

$$= W^{k^2/2} \sum_{n=0}^{N-1} g(n) W^{-(k-n)^2/2} \quad (3.4)$$

where  $g(n) = y(n)e^{-jw_0n}W^{n^2/2}$ .

Replacing  $k$  by  $n$  and  $n$  by  $k$  in Eq. 3.5 to obtain more familiar notation :

$$Y(e^{jw_n}) = W^{n^2/2} \sum_{k=0}^{N-1} g(k) W^{-(n-k)^2/2}, \quad n = 0, 1, \dots, M-1 \quad (3.5)$$

Define  $h(n) = W^{-n^2/2}$ ,  $-(N-1) \leq n \leq M-1$ , otherwise 0. Eq. 3.5 can be interpreted as the output of a linear time-invariant system,  $h(n)$ . Because the summation part of Eq. 3.5 is the convolution of  $g(n)$  and  $h(n)$ , one can apply FFT to it to reduce the computation complexity. Here, the FFT size is  $L = M+N-1$  so that the circular convolution will be equal to the linear convolution for  $0 \leq n \leq M-1$ . Thus,  $g(n)$  must be zero-padded to  $L$ . However,  $h(n)$  is noncausal, and for real-time implementations, it must be delayed by  $(N-1)$  to be a causal system,  $h'(n)$ . So, the computation of Eq. 3.5 is as depicted in Fig. 3.6.

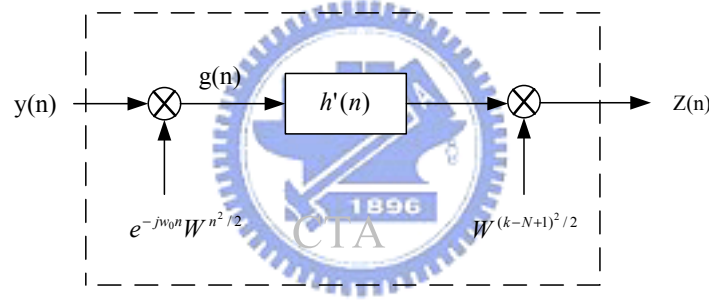


Fig. 3.6: Block diagram of CTA

The desired frequency samples are given by

$$Y(e^{jw_n}) = Z(n + N - 1), \quad n = 0, \dots, M-1 \quad (3.6)$$

### 3.2.2 CTA Method

Because using CTA can find certain  $M$  frequency samples from  $N$  ( $>M$ ) time samples, we can employ it to find the chosen range of the Doppler frequency,  $\hat{w}_r$ , from the carrier frequency,  $w_c$ , as discussed in section 2.4. Generally speaking, the selected range can be  $\hat{w}_r = -w_d \sim +w_d$ . The common FFT methods uses  $N$  time samples to find  $N$  frequency samples, which is limited to find fine frequency in our interested range. In other words, the frequency resolution of the common FFT methods depends on the length of sampled points



in time domain. To apply CTA to the acquisition problem of the carrier frequency, some parameters can be set in the following:

$$w_0 = w_b - w_d; \quad \Delta w = 2w_d/R_d \quad (3.7)$$

$\Delta w$  is the desired frequency resolution which is dependent on  $R_d$ .

Thus, replacing the FFT part by the CTA in Fig. 3.3 yields the block diagram Fig. 3.7.

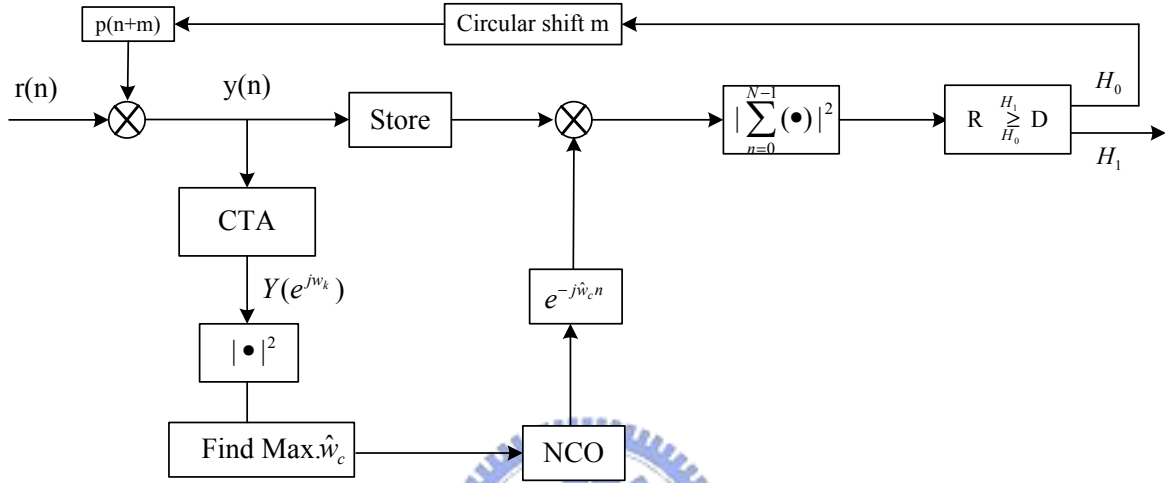


Fig. 3.7: Using CTA to estimate the Doppler frequency

To reduce the computation complexity, one can apply FFT to the convolution part of CTA as shown in Fig. 3.8.

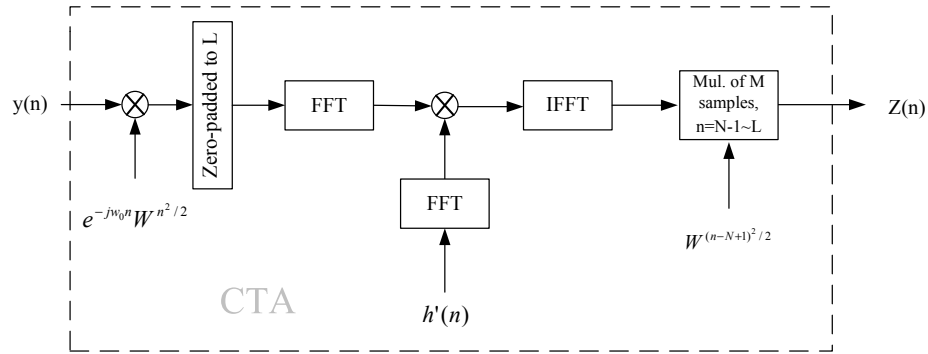


Fig. 3.8: Block diagram of CTA using FFT

### 3.2.3 Two-stage Search Strategy

The method introduced in the section 3.2.2 is still very tedious and time-consuming as a result of doing shifting 2152 half-chip times at the sampling frequency  $f_S = 2.1518$  MHz,

although we have the fine frequency resolution. And in the sections 3.1.1 and 3.1.2, even though P-S method has lower computation complexity than S-P method has, in order to get fine frequency resolution one still needs to change NCO many times. Thus, we propose a new strategy to use CTA to estimate the Doppler frequency and FFT to estimate the code delay. The acquisition is accomplished in two stages, and therefore we call it two-stage search strategy. The acquisition processes of this approach are similar to the double-dwell search strategy; two operations are required. However, from the realization viewpoint double-dwell search strategy is performed in time domain but our approach is in frequency domain. The detailed procedures are discussed below.

1) In the first stage, use the Parallel-Serial method to find the delay with only several Doppler frequency bins.

2) In the second stage, apply the obtained code delay from the first stage to find the fine Doppler frequency via CTA. The block diagram is shown in Fig. 3.9.

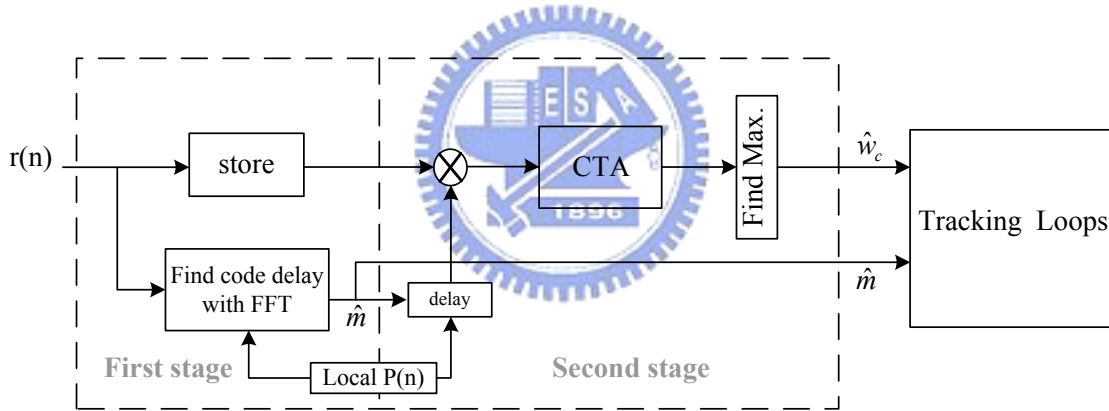


Fig. 3.9: Two-stage search strategy diagram

### 3.3 Computation Complexity

In order to measure the computation complexity of above methods, some assumptions are made. The length of FFT must be of radix 2. In the following discussions, the number of operations required to an FFT of length  $N$  is equal to  $(N \log_2 N)/2$  multiplications and  $N \log_2 N$  additions. All methods are compared with each other under the same frequency resolution and the equal range of Doppler frequency. The frequency resolution is  $\Delta f = f_r/(R_w - 1)$ , where  $f_r$  is the range of the Doppler frequency and  $R_w$  is the number of frequency bins. Define  $R_d$  be the number of code delays to be searched,  $N$  is the length of input signal in FFT methods, and  $N_i$  is the length of input signal in CTA method. Let  $N_c = N_i + M - 1$ . Assume that one multiplication and one addition is regarded as one operation.

In S-P method, the whole process of acquisition needs  $2NR_d + R_d R_w + R_d$  multiplications,  $NR_d$  additions, and  $R_d$  FFT operations.

The computation complexity of S-P method is

$$C_{sp} = R_d[3N + R_w + 1 + 3(N \log_2 N)/2]$$

In P-S method, it needs  $3R_w N$  multiplications and  $2R_w$  FFT operations.

The computation complexity of P-S method is

$$C_{ps} = 3R_w(N + 3N \log_2 N)$$

In CTA method using FFT, it needs  $3R_d N_i + R_d + R_w R_d$  multiplications,  $R_d N_i$  additions, and  $R_d$  CTA operations; one CTA operation needs  $N_i + N_c + R_w$  multiplications, and 2 FFT operations.

Thus, its computation complexity of CTA method is

$$C_c = R_d(5N_i + 1 + N_c + R_w + 3N_c \log_2 N_c)$$

In two-stage method with  $R'_w = (R_w - 1)/2 + 1$  frequency bins, its computation complexity is

$$C_t = 3R'_w(N + 3N \log_2 N) + N_i + N_c + R_w + 3N_c \log_2 N_c$$

The computation complexity of all discussed approaches are shown in Table 3.3. Here, we

	Computation complexity
S-P	$R_d[3N + R_w + 1 + 3(N \log_2 N)/2]$
P-S	$3R_w(N + 3N \log_2 N)$
CTA	$R_d(5N_i + 1 + N_c + R_w + 3N_c \log_2 N_c)$
Two-stage	$3R'_w(N + 3N \log_2 N) + N_i + N_c + R_w + 3N_c \log_2 N_c$

Table 3.1: Computation complexity of all

	Common parameters
The sampling frequency $f_s$	2.1518 MHz
The resolution of code delay	$T_s = \frac{1.023T_p}{2.1518}$
The range of Doppler frequency $f_r$	20 kHz
The frequency resolution $\Delta f$	131.33 Hz

Table 3.2: Common parameters

give a GPS application as a demonstrative example using the parameters shown in Table 3.3.

In S-P method, the length of input signal,  $N$ , must be chosen 16384, because  $N = f_s/\Delta f$ . The frequency bins is  $R_w = \lceil f_r/\Delta f \rceil = 153$ , where  $\lceil \cdot \rceil$  is the ceiling function. The number of code delays,  $R_d$ , is chosen as 2152 for less computation complexity. Thus, the computation complexity of S-P method is

$$\begin{aligned}
C_{sp} &= 2152 \times (3 \times 16384 + 153 + 1 + 3 \times 16384 \times 14/2) \\
&= 846,532,240
\end{aligned}$$

In P-S method, the length of input signal,  $N$ , is chosen as 4096 to be of radix 2 and over one period of C/A code. The number of frequency bins is  $R_w=153$ . The computation complexity of P-S method is

$$\begin{aligned}
C_{ps} &= 3 \times 153 \times (4096 + 3 \times 4096 \times 12) \\
&= 69,562,368
\end{aligned}$$

In CTA method, the length of FFT in CTA,  $N_c$ , must be of radix 2 and over one period of C/A code. Thus it can be chosen as 4096.  $N_i = N_c - R_w + 1 = 4096 - 153 + 1 = 3944$ .  $R_d$

can be chosen as 2152. The computation complexity of CTA method is

$$\begin{aligned} C_c &= 2152 \times [5 \times 3944 + 1 + 4096 + 153 + 3 \times 4096 \times 12] \\ &= 368,908,752 \end{aligned}$$

In two-stage method, at the first stage  $N$  can be 4096 and  $R'_w=77$ . At the second stage,  $N_i$  is the same, 3944, so  $N_c$  is 4096. The computation complexity of method two-stage is

$$\begin{aligned} C_t &= 3 \times 77 \times (4096 + 3 \times 4096 \times 12) + 3944 + 4096 + 153 + 3 \times 4096 \times 12 \\ &= 35,164,161 \end{aligned} \tag{3.8}$$

From the above example, one can find the order of computation complexity is method S-P > CTA > P-S > two-stage. As the frequency resolution increases, FFT methods will have more computation complexity than our methods. In comparison with S-P and CTA method, CTA does not only have the less computation complexity, but also has a shorter integration time than S-P method. In this example, the integration time of CTA is  $3944T_s$ , and that of S-P is  $16384T_s$ . It shows that the S-P method needs more time to collect the adequate data to make the frequency resolution high. However, in this way the SNR will be increased. Under lower SNR environments, the S-P method works more sensitively than CTA method to detect the wanted signal at the cost of a long collected data time. In comparison with P-S and two-stage method, two-stage method can have the less computation complexity.

## Chapter 4

# SIMULATIONS AND DISCUSSIONS

In this chapter, we show our simulations with the received signal, and 3-dimensional figures and 2-dimensional figures of uncertainty region. We use the same parameters in section 3.3. According to the characteristics of the real received signal, we use Matlab to simulate it. In the simulated received signal, the baseband frequency is set at  $f_b = 17.248$  kHz, the Doppler frequency is  $f_d = 3200$  Hz,  $f_c = f_b + f_d = 20.448$  kHz, and the code phase is set as  $1000T_s$ . As expected, the received signal looks like noise in Fig. 4.1.

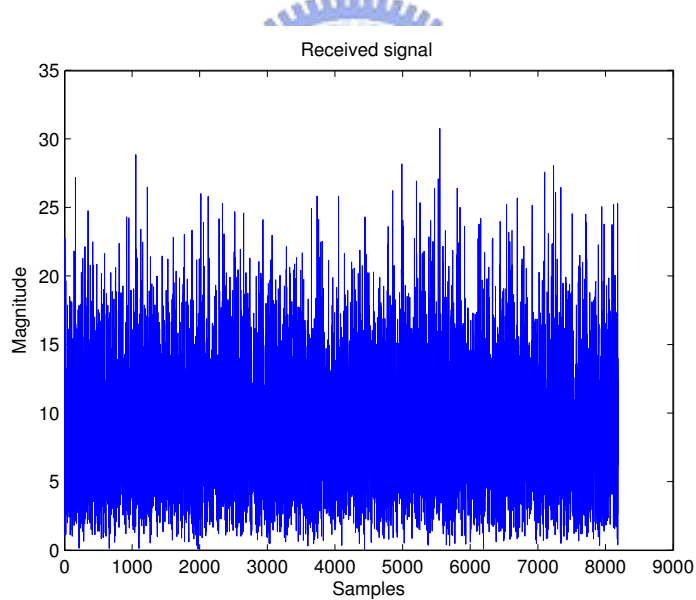


Fig. 4.1: Received signal in baseband from the satellite 12 with  $C/N_0 = 40$  dB-Hz

Three Figures 4.2, 4.3, and 4.4 are to show the simulation results of calculating the crosscorrelation of each cell to find the position of the maximum value (conventional method) with the 131.33 Hz frequency resolution and  $N = 2152$ . From Fig. 4.2, one may find a maximum peak at (102,1000).  $(102-1) \times 131.33 + 7.248$  kHz (the initial frequency)  $\approx 20.51$  kHz. The value is very close to  $f_c$ , so the signal is detected. For a clear view, a lateral view from the

Y direction and X direction are shown in Fig. 4.3, and 4.4.

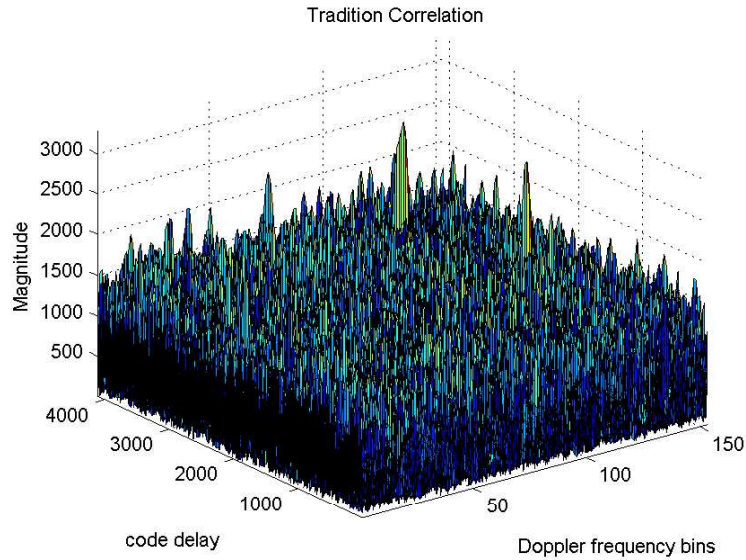


Fig. 4.2: Using the conventional method from the satellite 12 with  $C/N_0 = 40$  dB-Hz : 3-dimensional view

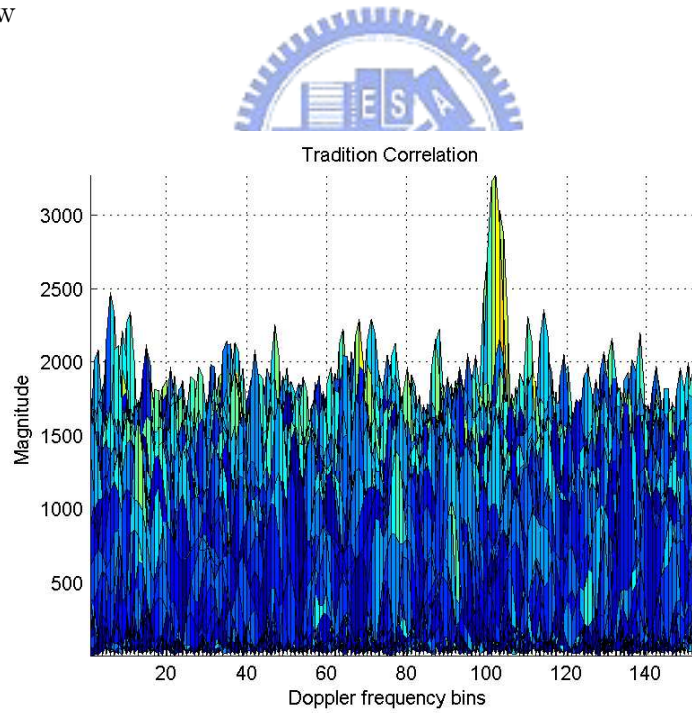


Fig. 4.3: Using the conventional method from the satellite 12 with  $C/N_0 = 40$  dB-Hz : lateral view

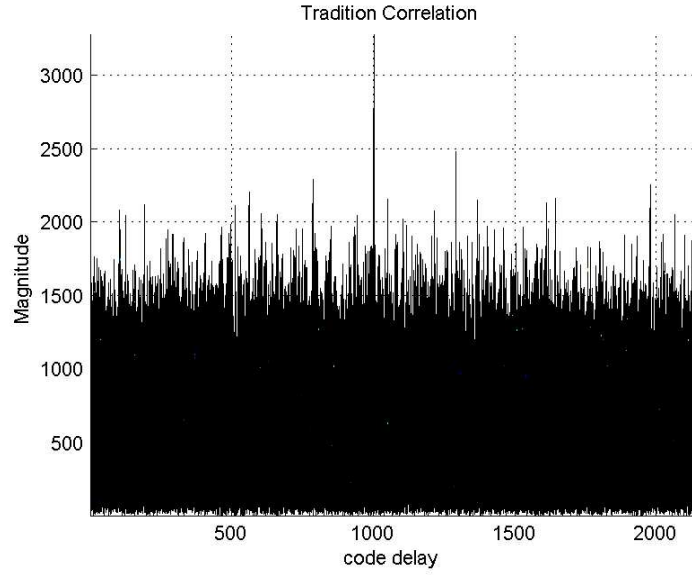


Fig. 4.4: Using the conventional method from the satellite 12 with  $C/N_0 = 40$  dB-Hz : lateral view 2

Three Figures 4.5, 4.6, and 4.7 are the simulation results of using FFT to find the Doppler frequency (S-P Method) with the 131.33 Hz frequency resolution,  $N = 16384$ , and  $R_d = 2152$ . According to these figures, the code delay can be found at 1000 in Fig. 4.7, and the frequency bin of the largest magnitude is located at 157 in Fig. 4.6.  $(157-1) \times 131.33$  Hz  $\approx 20.487$  kHz. It is very close to  $f_c$ .

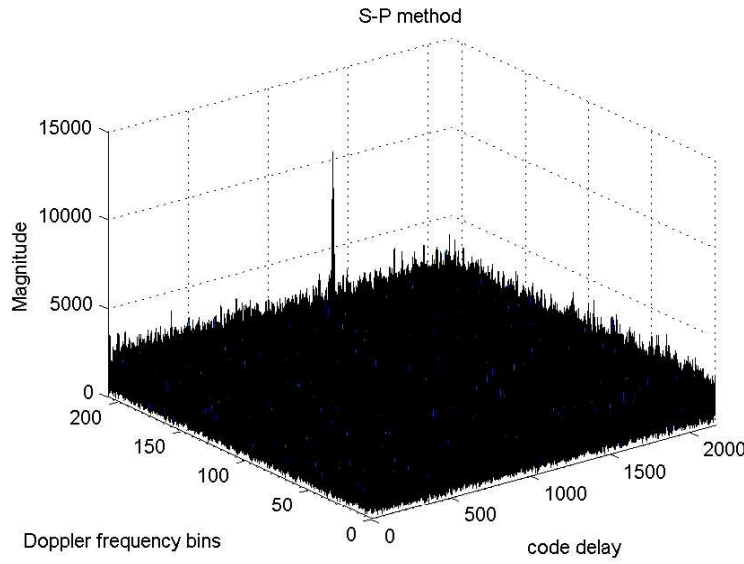


Fig. 4.5: Using FFT to estimate the Doppler frequency from the satellite 12 with  $C/N_0 = 40$  dB-Hz : 3-dimensional view



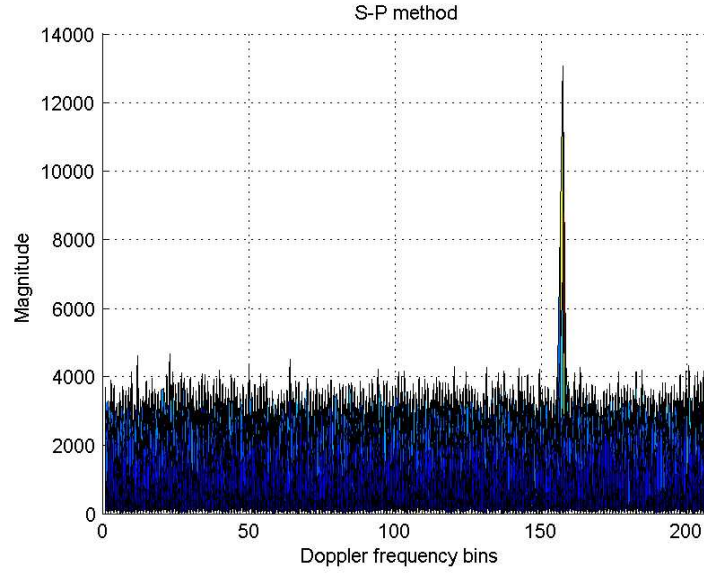


Fig. 4.6: Using FFT to estimate the Doppler frequency from the satellite 12 with  $C/N_0 = 40$  dB-Hz : lateral view

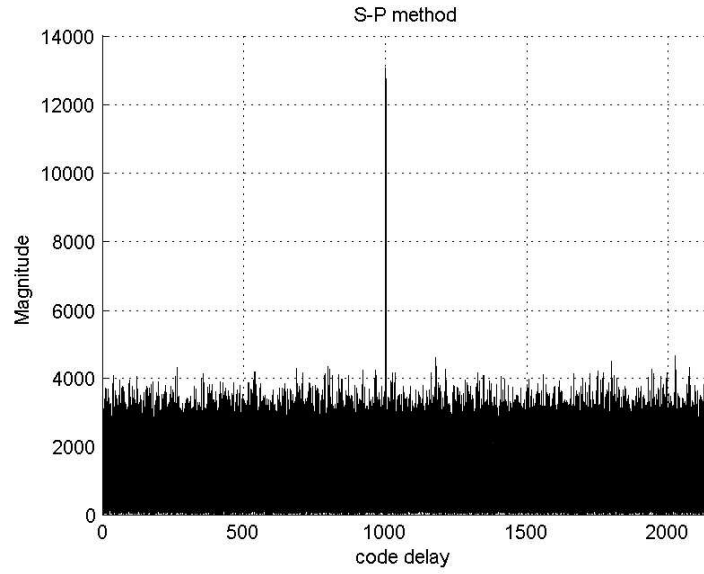


Fig. 4.7: Using FFT to estimate the Doppler frequency from the satellite 12 with  $C/N_0 = 40$  dB-Hz : lateral view 2

Three Figures 4.8, 4.9, and 4.10 are the simulation results of using FFT to estimate the code delay (P-S Method) with the 131.33 Hz frequency resolution,  $N = 4096$ ,  $R_w = 153$ . In Fig. 4.10, it is obvious to find the code delay located at 1000. In Fig. 4.9, the frequency bin of the largest magnitude is at 101.  $(102-1) \times 131.33 \text{ Hz} + 7.248 \text{ kHz} \approx 20.512 \text{ kHz}$ . The signal is also detected. One can find they are the same to Figures 4.2, 4.3, and 4.4. It is

similar to what we have discussed in section 3.1.2.

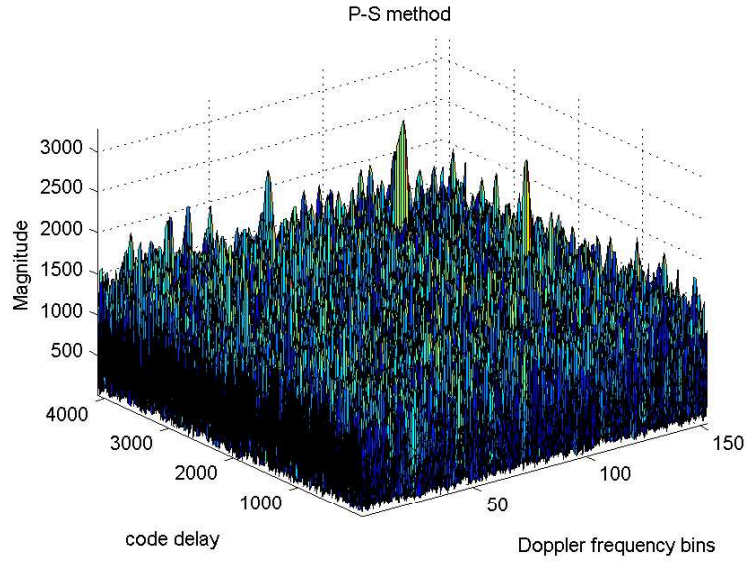


Fig. 4.8: Using FFT to estimate the code delay from the satellite 12 with  $C/N_0 = 40$  dB-Hz : 3-dimensional view

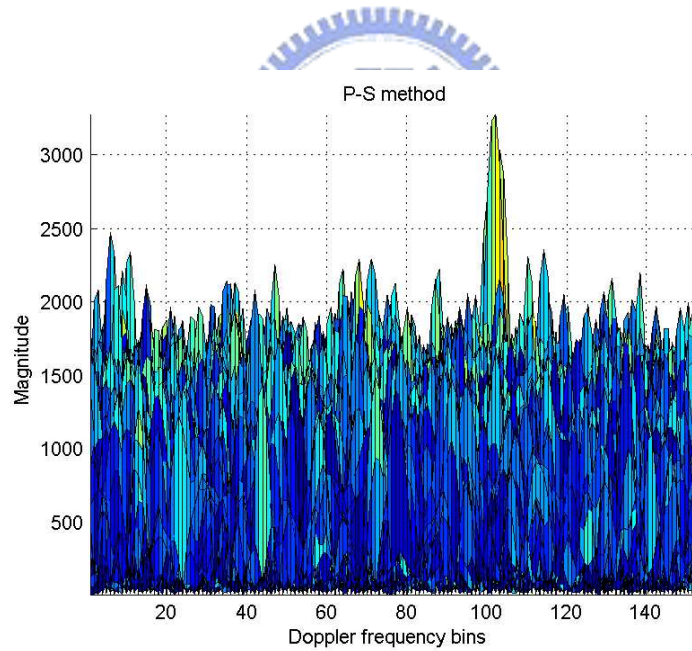


Fig. 4.9: Using FFT to estimate the code delay from the satellite 12 with  $C/N_0 = 40$  dB-Hz : lateral view

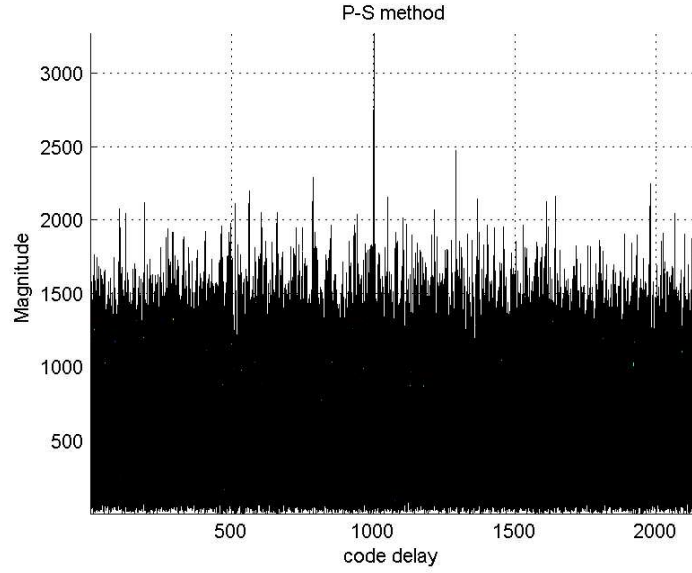


Fig. 4.10: Using FFT to estimate the code delay from the satellite 12 with  $C/N_0 = 40$  dB-Hz : lateral view 2

Three Figures 4.11, 4.12, and 4.13 are the simulation results of using CTA to estimate the Doppler frequency (CTA Method) with the 131.33 Hz frequency resolution,  $R_w = 153$ ,  $N_c = 4096$ , and  $R_d = 2152$ . One can find the frequency bin of the largest magnitude are at 102.  $(102 - 1) \times 131.33 \text{ Hz} + 7.248 \text{ kHz} \approx 20.512 \text{ kHz}$ . The code delay of the largest magnitude is at 1000. Therefore, we can claim the signal is detected.

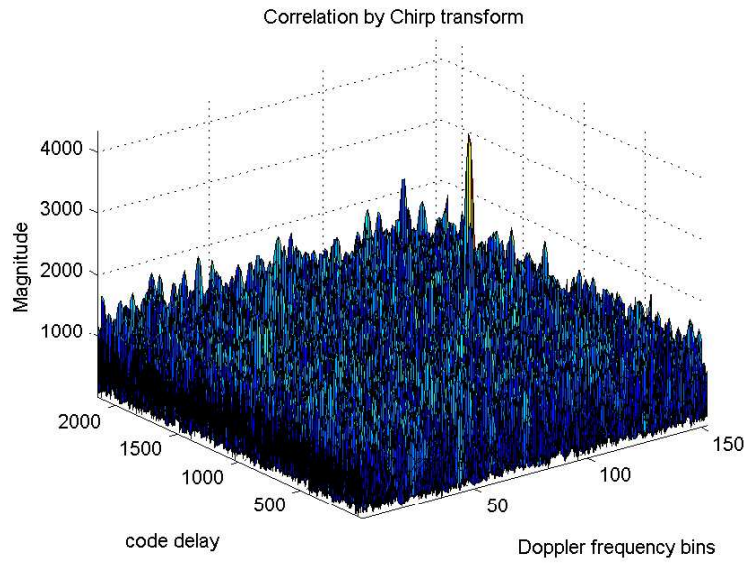


Fig. 4.11: Using CTA to estimate the Doppler frequency from the satellite 12 with  $C/N_0 = 40$  dB-Hz : 3-dimensional view

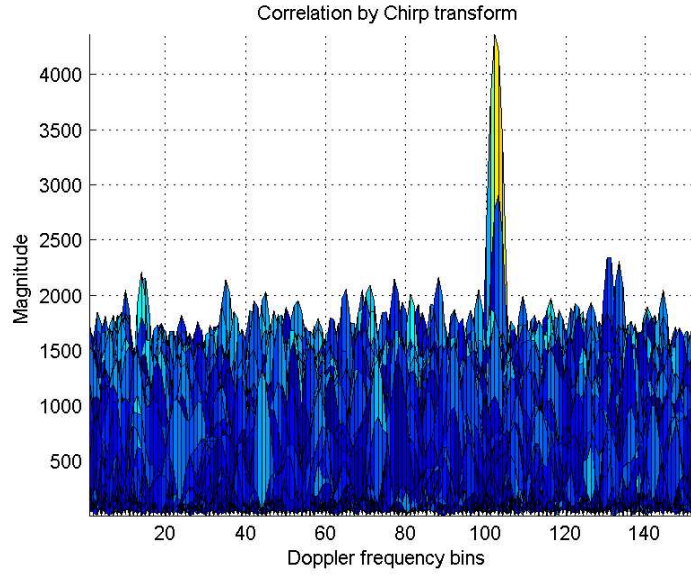


Fig. 4.12: Using CTA to estimate the Doppler frequency from the satellite 12 with  $C/N_0 = 40$  dB-Hz : lateral view

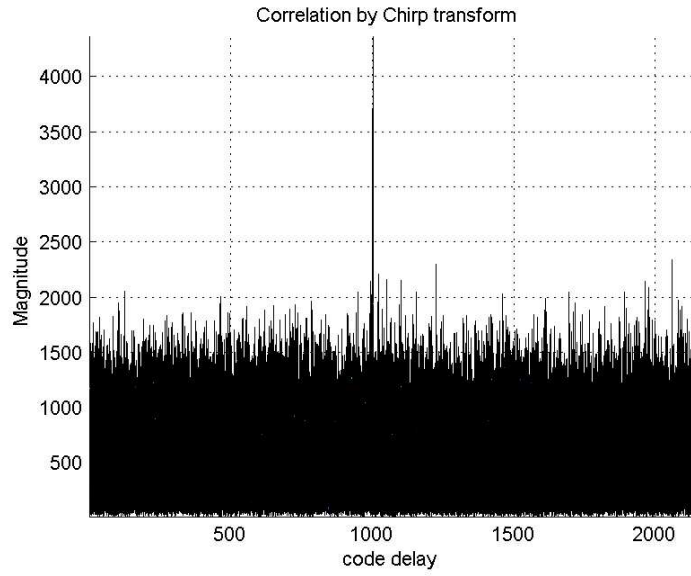


Fig. 4.13: Using CTA to estimate the Doppler frequency from the satellite 12 with  $C/N_0 = 40$  dB-Hz : lateral view 2

Four Figures 4.14, 4.15, 4.16, and 4.17 are using two-stage search method with the 131.33 Hz frequency resolution,  $R_w = 153$ . At first stage,  $N=4096$ , and  $R'_w=77$ . At second stage,  $N_c=4096$  and  $R_d = 2152$ . The first three Figures 4.14, 4.15, and 4.16 are the simulation results of first stage with coarse 77 frequency bins. In Fig. 4.16, the code delay is found at 1000. In the final Fig. 4.17, one can find there is a maximum peak at 102.  $(102-1) \times 131.33$

$\text{Hz} + 7.248 \text{ kHz} \approx 20.512 \text{ kHz}$ . Hence, two-stage successfully detects the signal.

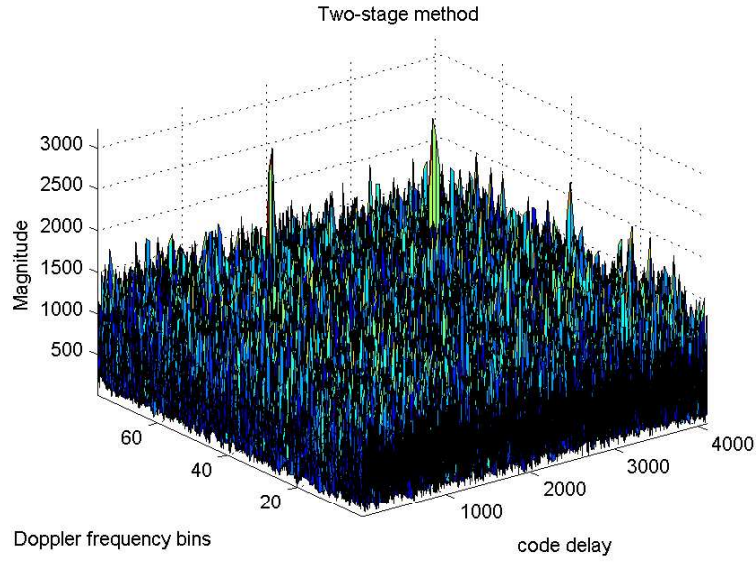


Fig. 4.14: Using two-stage search from the satellite 12 with 77 coarse frequency bins  $C/N_0 = 40 \text{ dB-Hz}$  : 3-dimensional view

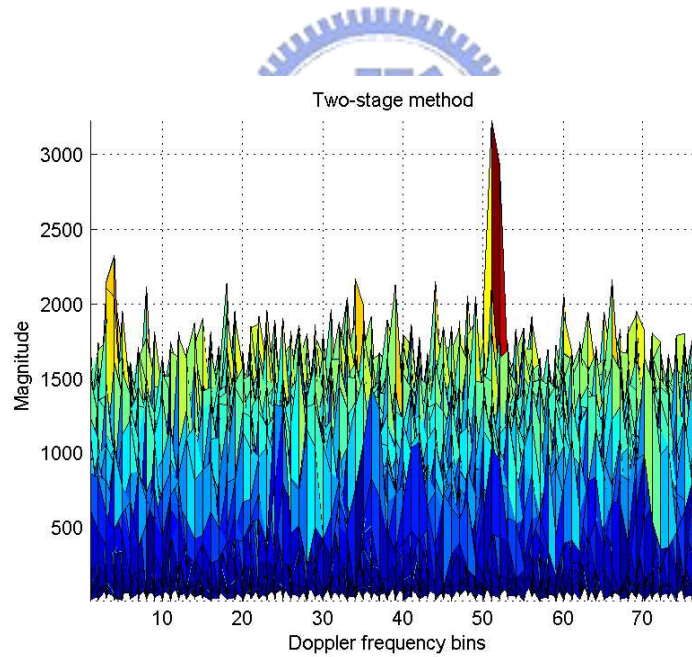


Fig. 4.15: Using Two-Stage search from the satellite 12 with 77 coarse frequency bins  $C/N_0 = 40 \text{ dB-Hz}$  : lateral view



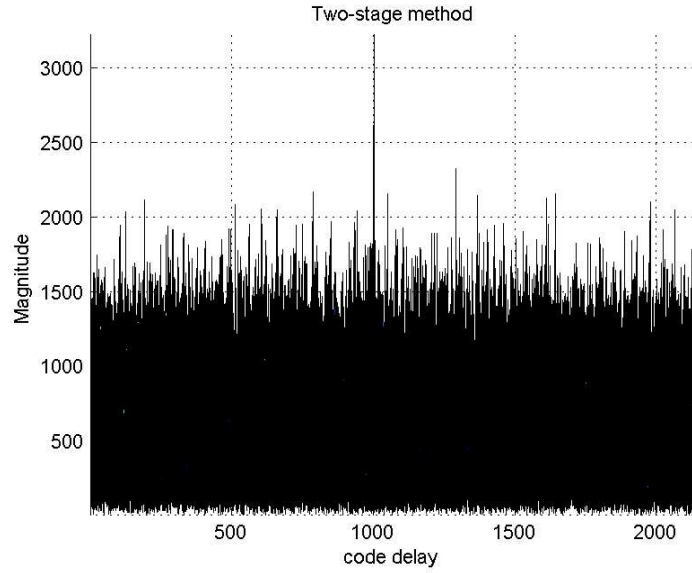


Fig. 4.16: Using Two-Stage search from the satellite 12 with 77 coarse frequency bins  $C/N_0 = 40$  dB-Hz : lateral view 2

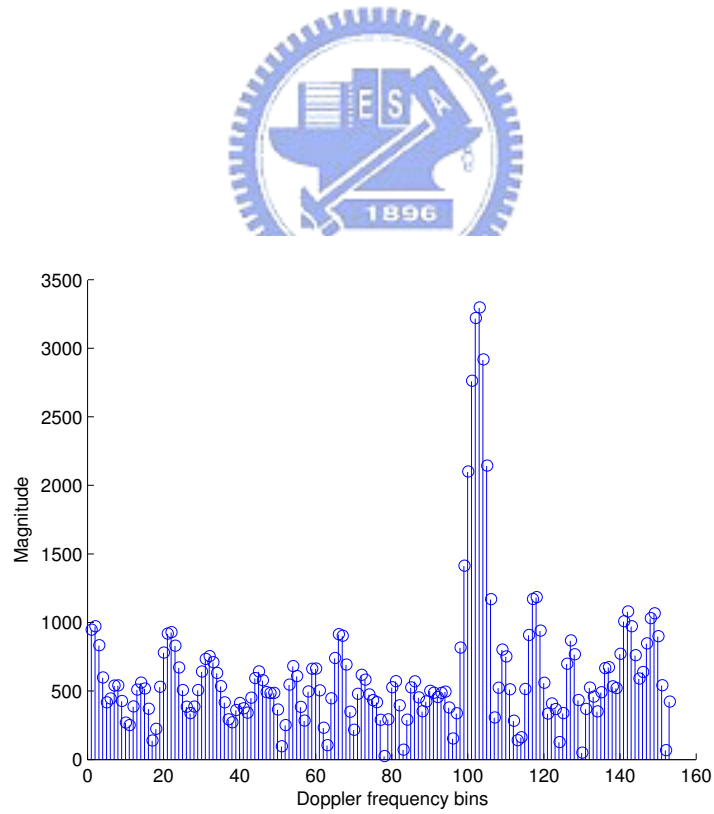


Fig. 4.17: Using CTA to estimate the Doppler frequency with the correct code delay from the satellite 12  $C/N_0 = 40$  dB-Hz

## Chapter 5

# CONCLUSIONS

In this thesis, the CTA is employed to develop an effective frequency-acquisition algorithm. Then, the two-stage method is presented such that the complexity for acquisition realization can be reduced. Computer simulations demonstrate further that for GPS applications the proposed methods perform satisfactorily with lower computation complexity under a wider range of the Doppler frequency. The proposed approach, naturally, is not limited to GPS applications, it can be applied to the acquisition applications of any communications via the direct sequence spread spectrum.



## REFERENCES

- [1] U. J. Cheng, J. H. William, and I. S. Joseph, "Spread Spectrum Code Acquisition in the Presence of Doppler Shift and Data Modulation," *IEEE Trans. Commun.*, Vol. 38, pp. 241-250, 1990.
- [2] D.J.R Van Nee, and A. J. R. M. Coenen, "New Fast GPS Code-Acquisition Technique Using FFT ," *IEE Electronics Letters*, Vol. 27, pp. 158-160, Jan. 1991
- [3] C. L. Spillard, S. M. Spangenberg, and G. J. R. Povey, "A Serial-Parallel FFT Correlator of PN Code Acquisition from LEO Satellites ," *Spread Spectrum Techniques and Applications, 1998. Proceedings., 1998 IEEE 5th International Symposium on* , Vol. 2, pp. 446-448, Sept. 1998
- [4] Y. F. Liu, Z. J. Chen, and S. L. Gus, "Implement and Performance Analysis of PN Code Acquisition Based on FFT," *Proceedings of the 5th World Congress on Intelligent Control and Automation*, pp. 5399-5401 June, 2004.
- [5] J. Starzyk and Z. Zhu, "Averaging Correlation for C/A Code Acquisition and Tracking in Frequency Domain," *IEEE MWSCS*, Fairborn, Ohio, Aug. 2001.
- [6] A. Alaqeeli, J. Starzyk, and F. Van Graas, "Real-Time Acquisition and Tracking for GPS Receivers," *Circuits and Systems, 2003. ISCAS '03. Proceedings of the 2003 International Symposium*, Vol. 4, pp. IV-500-IV-503, May 2003.
- [7] D. N. Fernaado and M. N. L. Jose, "A New Fast Code/Frequency Acquisition Algorithm for GPS C/A Signals," *Vehicular Technology Conference, 2003. VTC 2003-Fall. 2003 IEEE 58th*, Vol. 2, pp. 766-770, Oct. 2003.
- [8] J. B.-Y. Tsui, *Fundamentals of Global Positioning System Receivers, A Software Approach*, Wiley, New York, 2000.



- [9] “Global Positioning System Standard Positioning Service Signal Specification,” 2nd edition, *GPS Joint Program Office*, Jan. 1995.
- [10] W. H. Zhuang, “Composite GPS Receiver Modeling, Simulations and Applications,” Ph.D dissertation, Department of Electrical Engineering, University of New Brunswick, Fredericton, Oct. 1992.
- [11] W. H. Zhuang and J. Tranquilla, “Digital Baseband Processor for the GPS Receiver - Modeling and Simulations,” *IEEE Trans. on Aerospace and Electronic Systems*, Vol. 29, pp. 1343-1349, Oct. 1993.
- [12] W. J. Hurd, J. I. Statman, and V. A. Vilnrotter, “High Dynamic GPS Receiver Using Maximum Likelihood Estimation and Frequency Tracking,” *IEEE Trans. on Aerospace and Electronic Systems*, Vol. 23, pp. 425-437, July 1987.
- [13] A. V. Oppenheim, R. W. Schaffer, and J. R. Buck, *Discrete Time Signal Processing*, Prentice Hall International Editions, second edition, 1999.
- [14] J. B. Thomas, “Functional Description of Signal Processing in the Rogue GPS Receiver,” *JPL Publication*, 88-15, Pasadena, California, June 1988.
- [15] J. J. Spilker, “GPS Signal Structure And Performance Characteristics,” *Navigation, Institute of Navigation*, Vol. 25, No. 2, pp. 121-146, 1978.